A high-performance no-chamber fuel cell operated on ethanol flame

Kang Wang [a], Ran Ran [a], Yong Hao [b], Zongping Shao [a,*], Wanqin Jin [a], Nanping Xu [a]

[a] State Key Laboratory of Materials-Oriented Chemical Engineering, Nanjing University of Technology, No. 5 Xin Mofan Road, Nanjing 210009, PR China
[b] Mechanical Engineering, California Institute of Technology, Pasadena, CA 91125, United States

Abstract

A no-chamber solid-oxide fuel cell operated on a fuel-rich ethanol flame was reported. Heat produced from the combustion of ethanol thermally sustained the fuel cell at a temperature of 500–830 °C. Considerable amounts of hydrogen and carbon monoxide were also produced during the fuel-rich combustion which provided the direct fuels for the fuel cell. The location of the fuel cell with respect to the flame was found to have a significant effect on the fuel cell temperature and performance. The highest power density was achieved when the anode was exposed to the inner flame. By modifying the $Ni + Sm_{0.2}Ce_{0.8}O_{1.9}$ (SDC) anode with a thin Ru/SDC catalytic layer, the fuel cell envisaged not only an increase of the peak power density to $\sim$200 mW cm^{-2} but also a significant improvement of the anodic coking resistance.
© 2007 Published by Elsevier B.V.

Keywords: Flame fuel cell; Solid-oxide fuel cell; Ethanol; Ruthenium; $Sm_{0.2}Ce_{0.8}O_{1.9}$

1. Introduction

Fuel cells represent one of the cleanest, most efficient and most versatile technologies for chemical-to-electrical energy conversion [1]. Among the many types of fuel cells, solid-oxide fuel cells (SOFCs) have received considerable attention due to their high efficiency and fuel flexibility [2,3]. Conventional SOFCs are operated in a dual-chamber configuration (Fig. 1a), in which the cell is separated into two compartments with the help of sealant, with the anode chamber supplied with fuel and the cathode chamber with air. The dual-chamber SOFC does not require catalytically selective electrodes, since the electrodes are exposed to separate gas streams, and is generally considered to be the technology of choice for large-scale stationary power generation. However, normally the dual-chamber configuration is not considered suitable for portable applications in which frequent and rapid start-up and shut-down are necessary, due to large internal stress during the heating and cooling processes resulting from the thermal expansion mismatch between cell components and sealant.

More recently, the concept of a single-chamber solid-oxide fuel cell (SC-SOFC) has been proposed (Fig. 1b) [4–10]. It is a sealant-free configuration, with both electrodes exposed to the same premixed fuel–air mixture. The performance of the SC-SOFC depends on different catalytic selectivity of the anode and the cathode towards the fuel–oxidant mixture. Therefore, the anode and cathode materials must be carefully designed.

Very recently, the innovative concept of a direct-flame fuel cell, operated without a gas chamber, has also been proposed (Fig. 1c) [11,12]. Compared to the SC-SOFC, the flame fuel cell configuration is even simpler. The fuel-rich flame provides not only the fuel, but also the heat for thermally sustaining the fuel cell, with the result that external thermal management is unnecessary. The advantages of the direct-flame fuel cell include ultra-simple cell configuration and highly flexible fuel selection, since the structure of a fuel-rich flame is similar for all kinds of hydrocarbon fuels. Furthermore, as with the SC-SOFC, the direct-flame fuel cell is capable of rapid start-up and ideal for portable applications. However, the performance of the direct-flame fuel cell is still relatively poor [11,12], which hinders its practical applications.

On the other hand, ethanol is an ideal fuel, which is a non-toxic, renewable and easily reachable resource with high energy density and in liquid state at normal conditions. The application of ethanol as a fuel for fuel cell has attracted increasing attention

* Corresponding author. Tel.: +86 25 83587722; fax: +86 25 83365813.
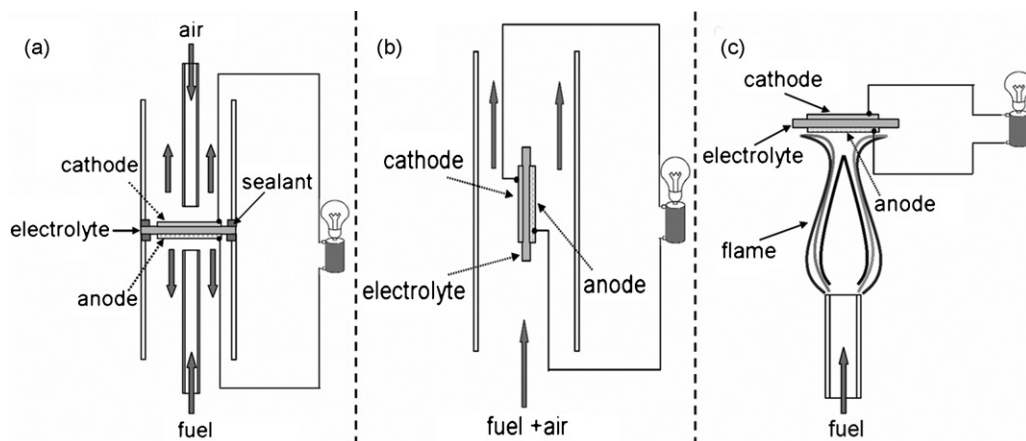E-mail address: shaozp@njut.edu.cn (Z. Shao).

Fig. 1. Schematic of fuel cells: (a) dual-chamber SOFC; (b) single-chamber SOFC; (c) flame fuel cell.

recently [13–18]. The direct ethanol fuel cell based on low-temperature polymer electrolyte membrane fuel cell (PEMFC) has been exploited in the past years [13–16]. In this paper, we report a coking-free flame fuel cell with improved anode by applying ethanol as fuel that doubled the performance as compared with ethanol fuel cell based on PEMFC. It may find potential applications in portable power generation.

2. Experimental

An electrolyte-supported fuel cell was used in this study. $Sm_{0.2}Ce_{0.8}O_{1.9}$ (SDC) was employed as the electrolyte material, which was prepared by a combined EDTA–citrate complexing sol–gel process [19]. Disk-shaped membranes with a diameter of 15 mm were prepared by dry pressing and sintered at 1350 °C for 5 h in air. Anode powder composed of NiO + SDC (60:40 w/w) was spray-deposited onto one central surface of the sintered electrolyte membrane with a rectangular shape and effective geometric surface area of 0.48 cm^2, followed by sintering at the same temperature for 5 h in air. The opposite surface of the membrane was symmetrically spray-deposited with a thin layer of $Ba_{0.5}Sr_{0.5}Co_{0.8}Fe_{0.2}O_{3-\delta}$ (BSCF) + SDC (70:30 w/w) composite and sintered at 1000 °C for 5 h in air. For some fuel cells, the anode surface was further screen-printed with a layer of Ru/SDC (8 wt.%) catalyst and fired at 800 °C in air. Table 1 shows the detailed fuel cell compositions and processing parameters. The surface morphologies of the fuel cells were observed by a scanning electron microscope (SEM, Quanra-2000). Shown in Fig. 2 are the typical cross-sectional morphologies of the cell.

An ethanol lamp was applied to provide the flame for the fuel cells. Fig. 3 shows a schematic of the fuel cell reactor. Here,
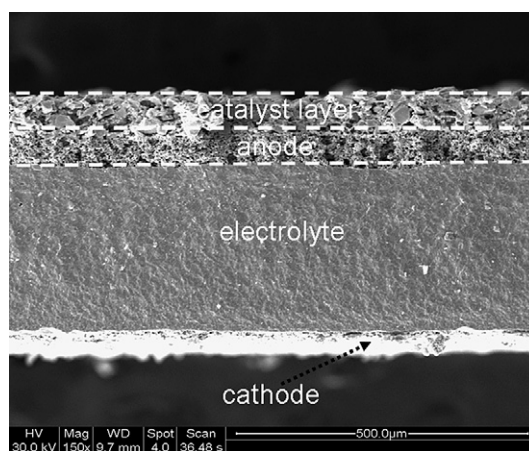

Fig. 2. The typical cross-sectional morphologies of the electrolyte-supported fuel cell with a Ru + SDC catalytic layer.

99.97% ethanol was used as the fuel, with a density of 0.79 g m^{-3} (20 °C). The burning rate of the ethanol flame was kept constant at 0.19 g min^{-1}. The fuel cell was located above the flame with the anode facing the flamefront and the cathode exposed to ambient air. Silver paste and silver wires were used as the current collector to minimize possible catalytic activity for ethanol reforming. A K-type thermocouple, penetrating into the flame or attached to the fuel cell surface, was used for measuring the apparent temperature inside the flame or fuel cell temperature. The fuel cell performance was tested by I–V characterization using a digital sourcemeter (Keithley 2420) interfaced with a computer for data acquisition.

The flame gases were sampled via a micro-tube for in situ composition analysis by a mass spectrometer (Hiden QIC 20).

Table 1
Detailed compositions, processing parameters and selected properties of the fuel cells

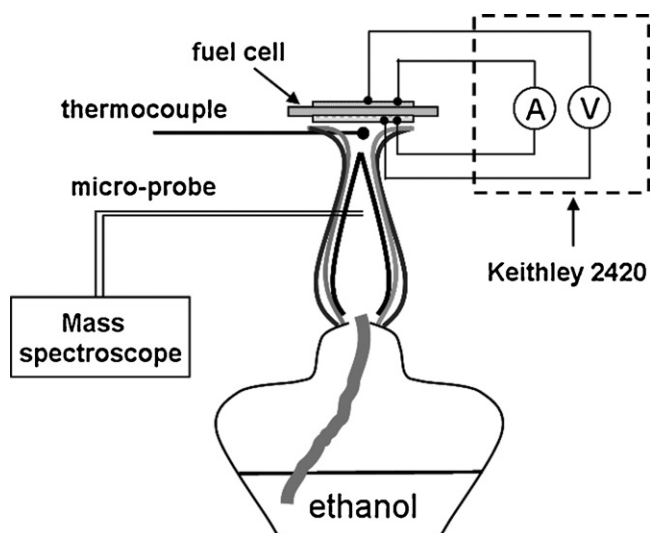| Components	Materials	Fabrication methods	Sintered temperature (°C)	Sintered time (h)	Thickness (μm)
Electrolyte	SDC	Dry pressing	1350	5	400
Anode	SDC + NiO	Spraying	1350	5	50
Cathode	BSCF + SDC	Spraying	1000	5	15
Catalytic layer	Ru/SDC	Screen printing	850	0.5	40

Fig. 3. Experimental setup for a direct-ethanol flame fuel cell.

The sampling rate was so small that it had negligible effect on the flame shape and composition. The mass spectrometer was pumped to a pressure of $\approx 1 \times 10^{-5}$ Torr using a turbomolecular pump. Water and ethanol were removed from the products before they reached the mass spectrometer in order to avoid poisoning. The micro-tube first sampled the ambient air for about 400 s before it quickly penetrated into the flame for flame composition analysis.

The peak at the mass-to-charge ratio of 2 in the mass spectrum was selected for detection of H_2. Although water and ethanol could also produce H_2^+ fragments, their contributions were negligible since they were removed before the gases entered the sampling tube. The peak at m/z of 44 was selected for the detection of CO_2. As to CO, since N_2 and CO have the same molecule weight of 28 and CO_2 could also produce a CO^+ fragment, we cannot simply take the peak at m/z of 28 to measure CO. In order to get the CO content from the peak at m/z of 28 (C_{det}), the contributions from N_2 and CO_2 must be subtracted. We know that the peak at m/z of 14 contributed from the characteristic fragment of N_2, i.e., N^+, which has a fixed relative intensity of 7.2% to that of N_2^+ at m/z of 28 for a pure N_2 gas. On the other hand,

the peak intensity of CO^+ from the cleaving of CO_2 is 11.4% that of CO_2^+ at m/z of 44 for a pure CO_2 gas. The CO content (C_{CO}) was then calculated as follows

$$C_{CO} = C_{det} - C_{N_2} - 0.114 C_{CO_2} \tag{1}$$

$$C_{N_2} = 100 \times \frac{C_N}{7.2} \tag{2}$$

where C_N is the detection content of N at m/z of 14, and C_{CO_2} is the detection content of CO_2 at m/z of 44, in mass spectroscopy, respectively.

3. Results and discussion

As shown in Fig. 4a, the ethanol flame is characterized by a three-layer structure with distinguished layer colors [20]. Across the flame from the center to outside, the layers are named as central flame, inner flame and outer flame, respectively. Different from the premixed fuel-air flame, the ethanol flame investigated here was created by an inter-diffusion of ethanol and oxygen. During the combustion, ethanol continuously diffused from the center of the flame to ambient atmosphere while oxygen diffused in the reverse direction. Positioning the fuel cell on top of the flame resulted in a change of the flame shape as shown in Fig. 4b.

A thermocouple was applied to probe the apparent temperature inside the flame at different positions with and without the fuel cell disk on top of the flame. It should be mentioned that temperature of a flame with a thermocouple is somewhat difficult, because of catalytic reactions on the thermocouple and to radiation corrections that have to be applied. The true temperatures of the flame gases are probably hundreds of degrees hotter.

As shown in Fig. 5, the flame temperature reached 500–830 °C, depending on the position in the flame. An increase in the temperature was observed across the flame from the center to the outside. Positioning the fuel cell on top of the flame resulted in a decrease of the temperature of about 10–30 °C. Such a decrease is easy to understand since the fuel cell increased the heat loss from surface radiation and also presents a physical barrier for oxygen diffusion. Interestingly, such a fuel cell
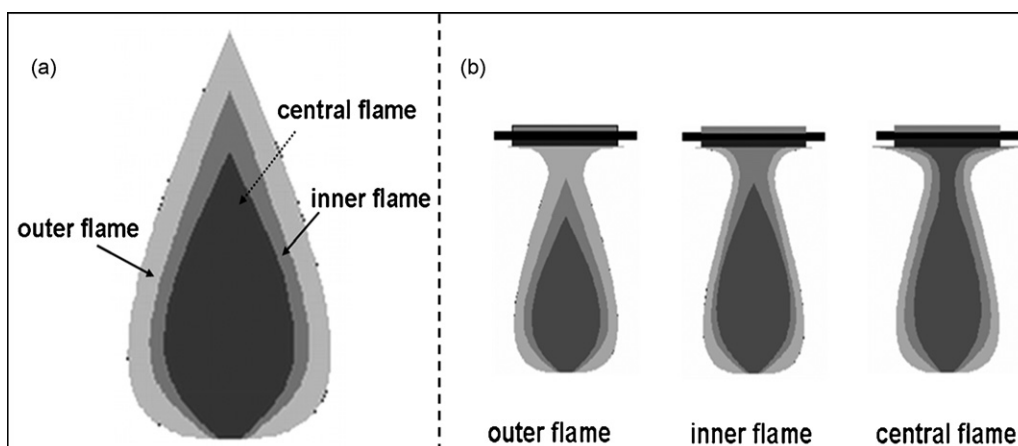

Fig. 4. Schematic of the shape of an ethanol flame: (a) without fuel cell and (b) with fuel cell over the flame at different positions.
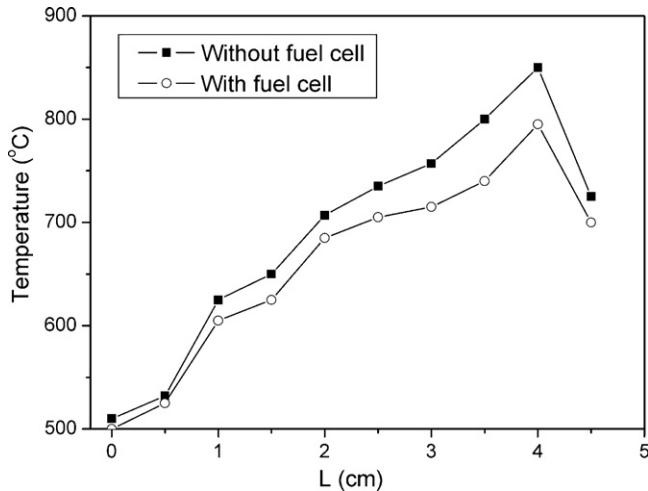
Fig. 5. Location-related temperature profiles with and without the fuel cell disk over the top of the flame.

temperature range was just ideal for operating the doped-ceria based electrolyte. Long-term stability test demonstrated that the cell temperature was stable if the ethanol combustion rate kept constant and there was no environmental disturbance, which suggests that the ethanol flame can be applied efficiently as a heater for thermally sustaining the fuel cell, which then omits

the requirement for external thermal management and greatly simplifies the fuel cell system.

Ethanol by itself can serve as a direct fuel for an SOFC; however, its partial oxidation products of syngas ($CO + H_2$) are far more active electrochemically. Another advantage of syngas over ethanol as a fuel is that the fuel cell anode is expected to be much less prone to carbon coking. Therefore ethanol reforming products are preferred as the fuels for SOFC. It is well known that the flame can work as a fuel reformer, and the approach of using fuel-rich flames for the production of synthesis gas via partial oxidation has been demonstrated by several authors, in particular with the help of porous combustors [21–23]. It was reported that the reaction products of a fuel-rich pre-mixed hydrocarbon flame consist of mainly N_2, CO_2, H_2O, CO and H_2 [24]. This is believed to be true for all kind of hydrocarbons including gaseous, liquid and solid fuels [12]. In this study, the inner and central flames of the ethanol flame could be considered as a fuel-rich flame with an increasing fuel-to-oxygen ratio across the flame from outside to center, and are therefore especially suitable for operating flame fuel cells.

In order to assess the nature of the fuel species available for the SOFC of the ethanol flame, the ethanol flame was sampled by a micro-quartz tube probe connected to a mass spectrometer, where the flame composition was analyzed. Fig. 6 shows the gas composition at positions about 1 cm (central flame), 2.4 cm
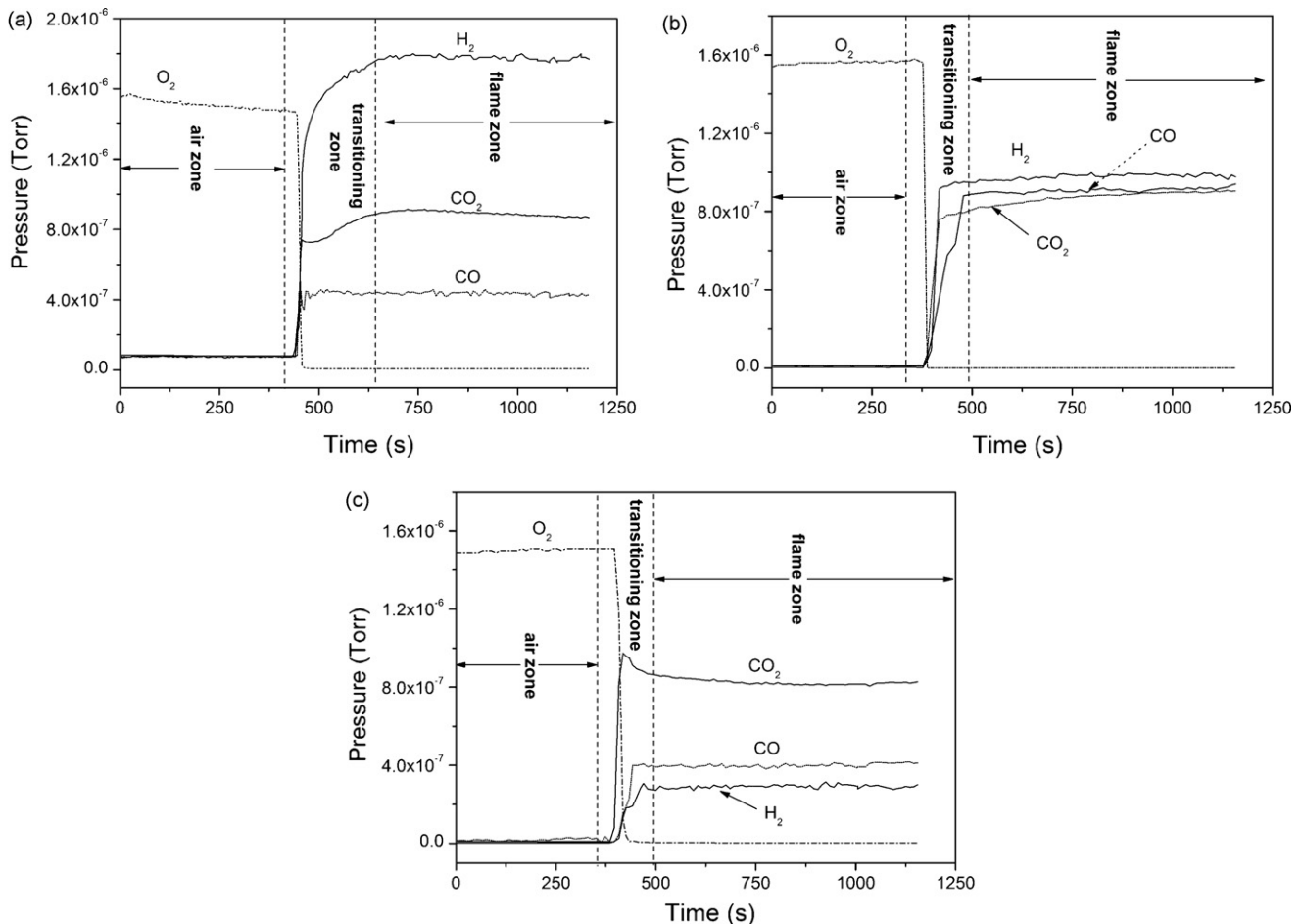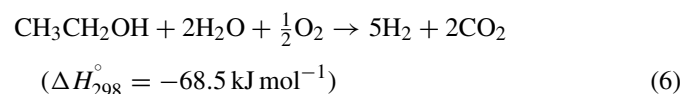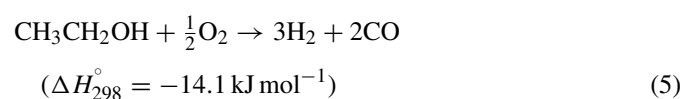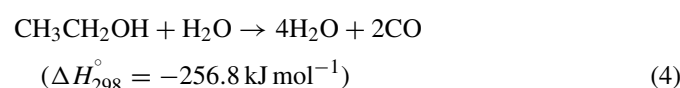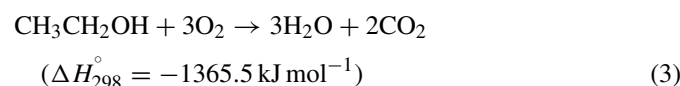

Fig. 6. Gas compositions of the flame at different positions: (a) central flame, (b) inner flame and (c) outer flame.

(inner flame) and 4.0 cm (outer flame) away from the center of the flame, respectively. "Air zone" and "flame zone" mean the zones at which mass spectrometer was sampling the air and the flame, respectively. The transitioning zone means the region in which the gas probed by the mass spectrometer changes from air to flame products. It clearly demonstrated there was a considerable amount of H_2 and CO produced within the flame at steady state. Therefore, the fuel-rich ethanol flame worked well as a fuel reformer in this study. Our measurement showed that the deeper into of the flame, the higher the H_2 concentration and the lower the CO_2 concentration, which can be explained by the increasing fuel-to-oxygen ratio across the flame.

During the ethanol combustion process many reactions are possible, including:

$$CH_3CH_2OH + 3O_2 \rightarrow 3H_2O + 2CO_2$$
$$(\Delta H_{298}^{\circ} = -1365.5 \, kJ \, mol^{-1}) \tag{3}$$

$$CH_3CH_2OH + H_2O \rightarrow 4H_2O + 2CO$$
$$(\Delta H_{298}^{\circ} = -256.8 \, kJ \, mol^{-1}) \tag{4}$$

$$CH_3CH_2OH + \tfrac{1}{2}O_2 \rightarrow 3H_2 + 2CO$$
$$(\Delta H_{298}^{\circ} = -14.1 \, kJ \, mol^{-1}) \tag{5}$$

$$CH_3CH_2OH + 2H_2O + \tfrac{1}{2}O_2 \rightarrow 5H_2 + 2CO_2$$
$$(\Delta H_{298}^{\circ} = -68.5 \, kJ \, mol^{-1}) \tag{6}$$

Deep oxidation of ethanol (Eq. (3)) produces a huge amount of heat, which accounts for the highest temperature of the outer flame where the oxygen concentration is the highest. Under fuel-rich condition, the combustion would be in favor of reactions (4)–(6), and consequently much more hydrogen is produced. A decrease in flame temperature could also be expected because of the reduction in heat release.

Once the SOFC was positioned over the ethanol flame with the anode facing the flame front, a positive open circuit voltage (OCV) was established in seconds while the fuel cell performance reached steady state in minutes. Fig. 7 shows the I–V curves of the fuel cells (stable performance) without and with the catalytic layer on top of the anode. For both cases, the OCVs experienced an increase with the fuel cell moving downwards from the outer flame to the central flame. An OCV of 0.65, 0.70 and 0.75 V was observed (Fig. 7(a)) for the fuel cell located over the outer, inner and central flames, respectively. Based on the results in Figs. 4 and 5, the increase in OCV should be mainly attributed to both the decrease in fuel cell temperature and the increase in fuel concentration over the anode side. At higher temperatures, the electronic conductivity of the SDC electrolyte becomes more significant, which results in the internal electronic shorting of the doped ceria electrolyte and consequently in a decreasing OCV. The maximum OCV (~0.75 V) observed in the current flame fuel cell was slightly higher than that obtainable in an SC-SOFC employing the same fuel cell components [5,6]. In the flame fuel cell, the cathode actually breathes the
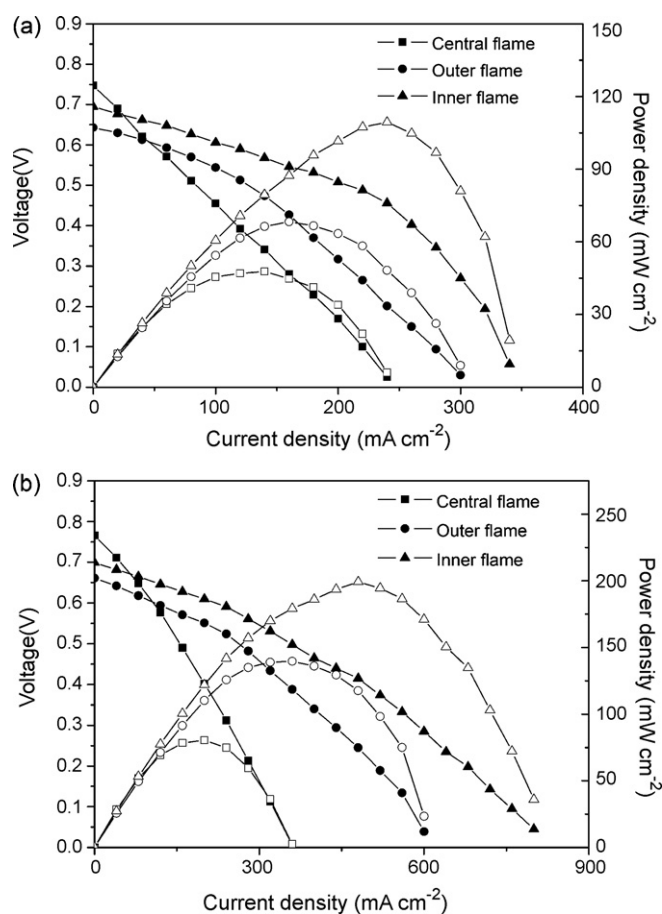

Fig. 7. The dependence of cell voltage and power density on current density of the fuel cells: (a) without and (b) with the catalytic layer on the top of the anode.

air, which ensures a higher oxygen partial pressure at the cathode than that in the SC-SOFC. In this sense, the flame fuel cell can be considered as a kind of internal reforming dual-chamber SOFC.

A peak power density of 45, 105 and 63 mW cm^{-2} was obtained for the fuel cell without the catalytic layer and with the anode facing the central, inner and outer flames, respectively. They are comparable to the results reported by other groups with methane-based flame-powered fuel cells [11,12]. Although the central flame had the highest concentration of hydrogen as shown in Fig. 6, it also had the lowest fuel cell temperature. The low cell temperature significantly reduced the electrode activity and increased the ohmic resistance of the electrolyte. On the other hand, the outer flame had the highest fuel cell temperature, but the hydrogen concentration was low due to the presence of a large amount of oxygen. Comparatively, the inner flame demonstrated the highest fuel cell performance since it had both an appropriate temperature and a favorable gas composition.

The OCV was only slightly improved when the anode surface was deposited with a thin catalytic layer. A value of 0.66, 0.71 and 0.77 V was obtained for the cases of outer, inner and central flames, respectively (Fig. 7(b)), which was only 0.02, 0.01 and 0.01 V higher than the case without the catalytic layer. However, the catalytic layer greatly enhanced the fuel cell performance, evidenced by a peak power density of 60, 200 and 130 mW cm^{-2}
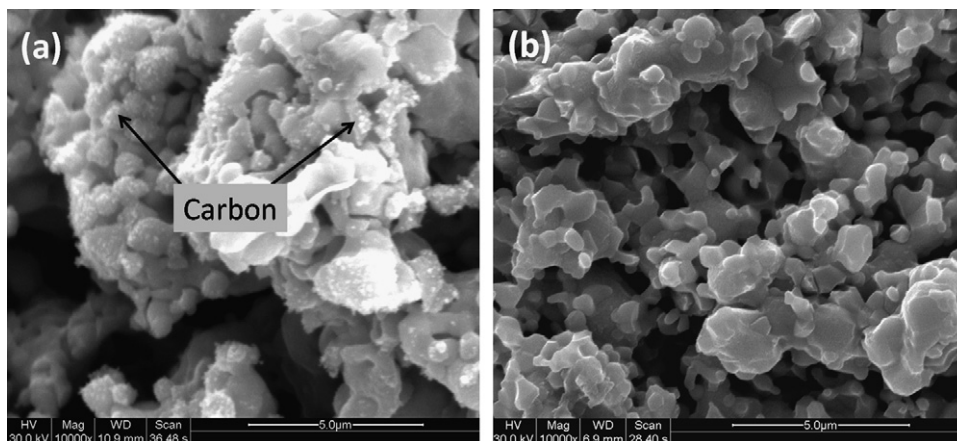
Fig. 8. SEM surface morphologies of the anode surface: (a) without and (b) with the Ru + SDC catalytic layer after test.

corresponding to the central, inner and outer flames, respectively. The significant improvement in performance could be due to the catalytic activity of the Ru/SDC catalytic layer towards ethanol reformation and partial oxidation. It is well known that the Ru/CeO$_2$-based catalysts have superior catalytic activities for hydrocarbon partial oxidation and reforming [25–27]. The deposition of the Ru/CeO$_2$-based catalyst over the anode might then promote the reactions (3)–(6). Kinetically, there should be a considerable amount of unreacted ethanol reaching the anode during the fuel cell operation after combustion. The Ru/SDC catalytic layer heterogeneously catalyzed the ethanol to syngas (CO + H$_2$) over the anode surface by reforming ethanol with the CO$_2$ and H$_2$O formed in situ or by partially oxidizing ethanol with the oxygen diffusing in from the ambient atmosphere. Due to the enhanced production of syngas, which is much more active electrochemically than ethanol, an increase in fuel cell performance should be expected.

By comparison with the SOFC in this study, the direct ethanol fuel cell based on polymer electrolyte membrane has also received increased attention due to the nontoxic and renewable characteristics of ethanol. However, up to now, its peak power density has been typically lower than 100 mW cm^2 [13–16]. Our data shows that the direct-flame SOFC in this study delivers a much better performance.

Despite the remarkable improvement in power density, coking remains a problem for the flame fuel cell in some cases. After an operation for more than 10 h, the anode was examined by SEM. Fig. 8 shows the SEM morphologies of the anode surface without and with the catalytic layer. Serious coking was observed over the fuel cell anode with bare Ni + SDC, which could be explained by the well-known fact that nickel catalyst promotes hydrocarbon cracking [28]. When Ru/SDC catalytic layer was applied however, the anode demonstrated no carbon deposition after the fuel cell test. This indicates that Ru/SDC greatly improved the coking resistance of the anode, and similar super coking resistant properties of the Ru/CeO$_2$-based catalytic layer have also been reported in literatures [29–31]. So we believe that this improved carbon-coking resistance of the anode is closely related to the capability of the ruthenium catalyst to promote the elimination of the carbon coking by the

following reaction:

$$C + H_2O \rightarrow CO + H_2 \tag{7}$$

4. Conclusions

The ethanol flame, which serves as a fuel reformer while at the same time providing the required heat for the fuel cell operation, was found to be an ideal power source for the flame fuel cells based on the SDC electrolyte. It was found that the fuel cell temperature and performance strongly depended on the location of the fuel cell with respect to the flame, and the performance decreased in the order of inner, outer and central flames for fuel cells both with and without the catalytic layer. A maximum power density of 200 mW cm^{-2} was achieved with the catalytic-layer-deposited anode exposed to the inner flame. The functional catalytic layer demonstrated beneficial effects on improving both the performance and the coking resistance of the fuel cell. Considering the high-performance and the ultra-simple configuration, the direct ethanol flame fuel cell reported here may have the potential for applications in portable power generation in future.

However, a few challenges remain for this type of fuel cells and need to be addressed by future research. (1) Thermal management. The uneven heating of the flame will induce the thermal stress within the fuel cell and may cause it to crack. (2) Fuel utilization. Most of the fuel is consumed by combustion and therefore the total electrical efficiency is low. (3) System design. Flames in real situations are generally hard to control and may often be unstable. Despite these challenges, flame fuel cells could find their potential applications in scenarios where the need for portable power generation overrides the requirement for high fuel utilization, and/or where heat and electricity co-generation is desired.

Acknowledgements

References

[1] B.C.H. Steele, A. Heinzel, Nature 414 (2001) 345–352.
[2] S.W. Tao, J.T.S. Irvine, Nat. Mater. 2 (2003) 320–323.
[3] S. Park, J.M. Vohs, R.J. Gorte, Nature 404 (2000) 265–267.
[4] T. Hibino, A. Hashimoto, Science 288 (2000) 2031–2033.
[5] Z.P. Shao, C. Kwak, S.M. Haile, Solid State Ionics 175 (2004) 39–46.
[6] Z.P. Shao, S.M. Haile, Nature 431 (2004) 170–173.
[7] T. Suzuki, P. Jasinski, V. Petrovsky, H.U. Anderson, F. Dogan, J. Electrochem. Soc. 151 (2004) 1473–1476.
[8] I.C. Stefan, C.P. Jacobson, S.J. Visco, L.C. De Jonghe, Electrochem. Solid State Lett. 7 (2003) 198–200.
[9] K. Wang, Z.P. Shao, Prog. Chem. 19 (2007) 267–275 (in Chinese).
[10] Z.P. Shao, J. Mederos, W.C. Chueh, S.M. Haile, J. Power sources 162 (2006) 589–596.
[11] M. Horiuchi, S. Suganuma, M. Watanabe, J. Electrochem. Soc. 151 (2004) 1402–1405.
[12] H. Kronemayer, D. Barzan, M. Horiuchi, S. Suganuma, Y. Tokutake, C. Schulz, W.G. Bessler, J. Power Sources 166 (2007) 120–126.
[13] G. Andreadis, P. Tsiakaras, Chem. Eng. Sci. 61 (2006) 7497–7508.
[14] E. Peled, T. Duvdevani, A. Aharon, A. Melman, Electrochem. Solid State Lett. 4 (2001) 38–41.
[15] C. Lamy, S. Rousseau, E.M. Belgsir, C. Coutanceau, J.-M. Léger, Electrochim. Acta 49 (2004) 3901–3908.
[16] J.R. Varcoe, R.C.T. Slade, E.L.H. Yee, S.D. Poynton, D.J. Driscoll, J. Power Sources 173 (2007) 194–199.
[17] B. Huang, S.R. Wang, R.Z. Liu, X.F. Ye, H.W. Nie, X.F. Sun, T.L. Wen, J. Power Sources 167 (2007) 39–46.
[18] S.L. Douvartzidesa, F.A. Coutelierisa, A.K. Deminb, P.E. Tsiakarasa, Int. J. Hydrogen Energy 29 (2004) 375–379.
[19] W. Zhou, Z.P. Shao, W.Q. Jin, J. Alloys Compd. 426 (2006) 368–374.
[20] Y.Y. Qian, J.B. Chen, Z.Z. Wu, R.Y. Wang, J.H. Xu, Chin. J. Chem. Educ. 24 (2003) 39–41.
[21] F.J. Weinberg, T.G. Bartleet, F.B. Carleton, P. Rimbotti, Combust. Flame 72 (1988) 235–239.
[22] D. Trimis, F. Durst, Combust. Sci. Technol. 121 (1996) 153–168.
[23] W.M. Mathis Jr., J.L. Ellzey, Combust. Sci. Technol. 175 (2003) 825–839.
[24] H. Pedersen-Mjaanes, L. Chan, E. Mastorakos, Int. J. Hydrogen Energy 30 (2005) 579–592.
[25] S. Hosokawa, S. Nogawa, M. Taniguchi, K. Utani, H. Kanai, S. Imamura, Appl. Catal. A 288 (2005) 67–73.
[26] L. Oliviero, J. Barbier Jr., D. Duprez, H. Wahyu, J.W. Ponton, I.S. Metcalfe, D. Mantzavinos, Appl. Catal. B 35 (2001) 1–12.
[27] Z.P. Shao, S.M. Haile, J. Ahn, P.D. Ronney, Z. Zhan, S.A. Barnett, Nature 435 (2005) 795–798.
[28] B.C.H. Steele, Solid State Ionics 86–88 (1996) 1223–1234.
[29] K. Wang, R. Ran, Z.P. Shao, J. Power Sources 170 (2007) 251–258.
[30] Z.L. Zhan, S.A. Barnett, Science 308 (2005) 844–847.
[31] T. Hibino, A. Hashimoto, M. Yano, M. Suzuki, M. Sano, Electrochim. Acta 48 (2003) 2531–2537.